EUR-CEA-FC-1579

Snake-like phenomena In Tore Supra following pellet injection

A.L. Pecquet, P. Cristofani, M. Mattioli, X. Garbet,
L. Laurent, A. Géraud, C. Gil, E. Joffrin, R. Sabot.

July 1996

CEA EURATOM

ASSOCIATION EURATOM-C.E.A.
DEPARTEMENT DE RECHERCHES
SUR LA FUSION CONTROLEE
C.E.N./CADARACHE
13108 SAINT PAUL LEZ DURANCE CEDEX

DRFC/CAD EUR-CEA-FC-1579

Snake-like phenomena In Tore Supra following pellet injection

A.L. Pecquet, P. Cristofani, M. Mattioli, X. Garbet,
L. Laurent, A. Géraud, C. Gil, E. Joffrin, R. Sabot.

July 1996

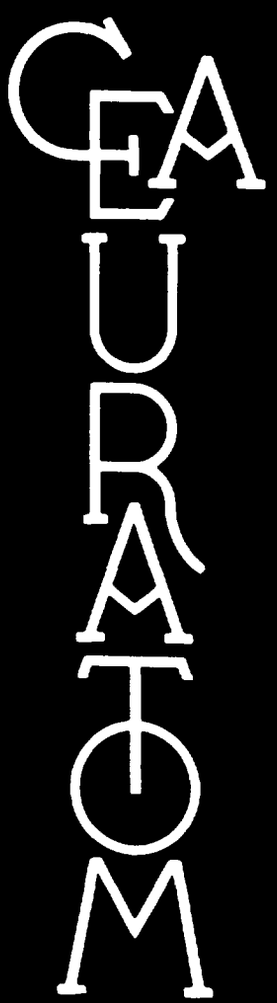

ASSOCIATION EURATOM-C.E.A.
DEPARTEMENT DE RECHERCHES
SUR LA FUSION CONTROLEE
C.E.N./CADARACHE
13108 SAINT PAUL LEZ DURANCE CEDEX

SNAKE-LIKE PHENOMENA IN TORE SUPRA FOLLOWING PELLET INJECTION

PECQUET A.L., CRISTOFANI P., MATTIOLI M., GARBET X., LAURENT L.
GERAUD A., GIL C., JOFFRIN E. and R. SABOT.

Association Euratom-CEA sur la Fusion
Département de Recherches sur la Fusion Contrôlée
CEN-Cadarache, F-13108 St Paul-lez-Durance

ABSTRACT

Snakes are observed in Tore-Supra, after injection of high velocity solid hydrogen or deuterium pellets ablated inside the q=1 surface. They are detected, immediately after the ablation, as oscillations on the line integrated densities of the central interferometer channels. The corresponding oscillations on the soft X-ray signals detach from the noise about 70 ms later. Snakes survive sawtooth crashes, but are nevertheless affected by them. Variations, during the about 500 ms long lifetime, of the snake radius r_s, of the rotation frequency and of the rotation direction are discussed, stressing the effects of the sawtooth crashes. In many snakes $r_s/r_{q=1}$ is of the order of 0.5. Since the snake has a m=1, n=1 helicity, this points out the existence of a flat or inverted safety factor profile, confirmed by calculation of the current profile using Spitzer's resistivity. Combined simulations of the snake oscillations on both interferometer and soft X-ray signals have indicated that, starting about 80 ms after the snake formation, the impurity (carbon) density inside the snake is much larger than outside it. Since a change of regime seems to appear about 80 ms after the snake formation on the soft X-ray, it seems plausible that impurity (carbon) accumulation takes place at this time. A stability criterion taking into account both impurity and bootstrap effects is presented, the result agrees with the model proposed by Wesson.

1. INTRODUCTION

Following the injection of high speed solid deuterium or hydrogen pellets reaching the q=1 surface, long lived small regions of high electron pressure have been first observed in JET [1] and subsequently in ASDEX [2]. They appear as regions of enhanced soft X-ray emission with a m=1, n=1 helicity and are called "snakes" from their snakelike shape on the soft X-ray camera time-space plots. A necessary but not sufficient condition for producing snakes is that the pellet crosses the q=1 surface. Analysis of the soft X-ray data together with information on the electron density n_e and temperature T_e (from laser interferometry and electron cyclotron emission, respectively) [3] have shown that snakes have perturbed parameters, relative to their surrounding: positive $\delta n_e/n_e \approx 25$ to 140% and negative $\delta T_e \approx 0$ to 200 eV, the latter being, however, not visible anymore at times greater than 100 ms after the snake creation. From a simplified quantitative expression of the soft X-ray emissivity (considering simply, as far as impurities are concerned, the enhancement factor ζ of a pure hydrogen plasma), it has been deduced [3] that the impurity concentration in the snake is larger than in the surrounding plasma. In JET, spontaneous snakes have also been observed immediately after the onset of sawteeth in discharges exhibiting impurity accumulation at early times [3], as well as, occasionally after pellet injection, "negative" snakes i.e. with reduced soft X-ray emission [4]. Recently, Wesson [5] has tried to analyse the snake formation and persistence on the basis of the growth and sustainement of a magnetic island.

Snakes are observed in Tore-Supra after high speed solid hydrogen or deuterium pellet injection during ohmic discharges as well as during discharges heated by ion cyclotron resonance (ICR) waves. Preliminary results have been already reported [6]. A more thorough discussion of the available Tore-Supra data on snakes is the purpose of this paper, which is organised as follows. In Section 2, the experimental observations are presented with particular attention to the "magnetic properties" of snakes, for example their localisation with respect to the q=1 surface and the influence of sawteeth. Since the snake rotates on a radius smaller than the radius of the q=1 surface (deduced from the sawtooth inversion radius), and since it has a m=1, n=1 helicity, the current density and q profiles following pellet injection are also considered in this Section . In Section 3 the snake "chemical" composition is obtained with a simplified model, simulating the oscillations of both the line integrated electron densities and the soft X-ray brightnesses. These simulations give, respectively, the electron and the carbon densities in the snake. The snake observations compared with the model recently proposed by Wesson [5] and the stability criterion taking into account both impurity and bootstrap effects are presented in Section 4, before the final discussion in Section 5.

2. GENERAL OBSERVATIONS

The results obtained up to now on Tore-Supra with a pneumatic high speed pellet injector are summarised in Ref.[7]. Hydrogen or deuterium pellets are formed by "in situ" condensation in the gun barrel, where they are accelerated. Velocities up to 3300 m/s are obtained with peak pressures higher than 1000 bars, driven by a two stage light gas gun. Depending on the plasma electron temperature, ablation takes place at or inside the q=1 surface for pellet speeds of the order of or higher than 1500 m/s. At the crossing of the q=1 surface, there is a large drop in the pellet ablation rate, this effect is associated with the reduced reservoir of hot electrons available for ablating the pellet within the resonant flux tube [8, 9]. In ohmic plasmas, for such high speeds, snakes are produced in about 50% of the cases. The striking observation is that, in contrast with JET results [3], in Tore-Supra the snakes are usually localised clearly inside the q=1 surface inferred from the sawtooth inversion radius. In some cases, snakes are formed early after the pellet ablation, but they decay away when the plasma shifts to a pellet enhanced performance (PEP) regime. The latter stops about 200 ms later and large m=1, n=1 oscillations appear during 30-40 ms. Impurity (carbon) accumulation inside the rotating island is necessary to simulate these m=1, n=1 modes in the same way as done for the snake (see Section 3).

2-a Snake description

As an example, an ohmic deuterium plasma (#12650) is considered with the following parameters: plasma current I_p = 1.4 MA, toroidal magnetic field on the magnetic axis B_Φ = 3.05 T, safety factor at the edge q_Ψ = 3.3, plasma minor a_L and major R radii equal, respectively, to 0.78 and 2.34 m. Prior to the injection, the central electron density $n_e(0)$ and temperature $T_e(0)$ are, respectively, equal to 3.3 10^{19} m^{-3} and 2.5 keV. The pellet, composed of about 10^{21} hydrogen atoms, is injected at a speed of 1550 m/s. In such experimental conditions, the penetration depth is equal to 0.63 m. Immediately after the injection, the central density and temperature become, respectively, equal to 1.25 10^{20} m^{-3} and 0.6 keV.

The snake is observed using data from the following diagnostics: 5 channels of the laser interferometer, 44 channels of the soft X-ray camera viewing the plasma vertically and 6 ECE channels of the Fabry-Perot interferometer giving the spatial profile of the electron temperature. Figure 1a shows (from top to bottom) the evolution during the snake lifetime of one ECE signal, two soft X-ray brightnesses and two integrated line densities as functions of time. One of the two soft X-ray detectors monitors the snake, viewing the intersection of the snake with the equatorial plane on the low magnetic field side (outwards). The other, viewing the region outside the q=1 surface, monitors the

inverted sawteeth. The ECE signal monitors the central T_e. The two interferometer channels cross the plasma on opposite sides with respect to the magnetic axis.

The early appearance of the modulations on the density indicates that the snake has already been created at the end of the ablation process, at t = 8.56 s. The amplitude of the perturbation is almost constant during the snake duration, at a level of the order of 5 to 6% of the line integrated density. The modulations on the increasing (because of the electron temperature recovery) soft X-ray signals appear only about 80 ms later, reaching a maximum of 150% relatively to theunperturbed signal around t = 8.85 s and then decreasing with a time constant of 170 ms. Fig1b shows, as a reference, the central line integrated density and the time evolution of the Fabry-Perot signal looking at the snake radius. The latter exhibits modulations of about 100 eV only visible at the beginning of the snake. The phase between the electron temperature and the line integrated density implies that the snake is cooler than the surrounding plasma. Both interferometric and soft X-ray modulations continue with variable frequency up to t ≈ 9.05 s, i.e., the snake lifetime is of the order of 500 ms. At t ≈ 8.65 s the snake contains approximately 5.5 10^{19} atoms representing 5% of the initial pellet. This result is deduced from a detailed analysis of the electron density during one snake rotation. As a matter of fact, as discussed in the following, the snake evolution is perturbed by the sawteeth, but survives to several crashes.

The opposite phase shifts, with respect to the magnetic axis of the density and soft X-ray oscillations determine a m=1 structure for the snake. This appears even more clearly when a biorthogonal decomposition (described in Ref.[10]) is applied to the soft X-ray signals. This decomposition, which is appropriate for the investigation of fluctuation phenomena, splits the signals into orthogonal spatial and temporal eigenfunctions, respectively called topos and chronos. Proceeding in the same way as in Section 4 of Ref. [10], the mode structure is inferred. In Figure 2 the first two k=1 and k=2 topos and chronos are shown as functions, respectively, of a spatial coordinate (the intersection of the viewing chords with the equatorial plane) and of time. The k=1 topo shows the spatial structure of the component of the signals with a slow time evolution, whereas the k=2 topo has the characteristic shape of a m=1 mode for which the abscissae of the maximum and of the minimum correspond to the two detectors viewing the intersection of the snake with the equatorial plane. These abscissae determine the mean value of the snake minor radius, $r_S = 0.14 \pm 0.015$ m, during its survival. The k=1 chrono is sensitive to the sawtooth (not clearly visible since they are quite weak), whereas the k=2 chrono shows only the fast fluctuations, from which the amplitude and rotation frequency of the mode can be obtained. The toroidal mode structure of the snake is obtained from the phase shifts of diagnostics located in different toroidal locations. Taking into account that the interferometer and the soft X-ray camera are

separated toroidally by 60°, the phase shift between them indicates a n=1 structure. Therefore, during its entire lifetime the snake is a perturbation of m=1, n=1 helicity, whose maximum takes place at $r_S = 0.14 \pm 0.015$ m.

The geometrical parameters characterising the snake dimensions are its minor radius r_S, a radial dimension l_r and a poloidal dimension l_θ. They can be obtained from the time evolutions of the suitable soft X-ray channels. The snake dimensions are given as full widths at half-maximum. Its structure between 8.85-8.95 s is sketched in Figure 3, with $r_S = 0.14$ m, $l_r = 0.12$ m, $l_\theta = 0.15$ m. A low/high field side asymmetry, connected to the Shafranov's shift is observed on the dimensions of the snake: $l_r = 0.15$ m on the high field side and $l_r = 0.12$ m on the low field side.

2-b Snake and sawtooth

The time evolutions in Figure 1 show that sawteeth are clearly distinguishable on soft X-rays 170 ms after the pellet injection, but on the central ECE data only after a delay of about 500 ms, i.e. about at the snake disappearance. This can be explain by the lower spatial resolution and the lower sensitivity of the Fabry-Perot interferometer with respect to the soft X-ray camera. On the other hand, when no snake is produced, sawteeth are visible on the ECE signals immediately after the injection.

The sawtooth inversion radius indicates a q=1 surface radius $r_{q=1} = 0.29 \pm 0.015$ m, which is the same as the one found before the injection. Figure 4 details this evaluation, showing the time evolutions during two sawtooth periods of three diodes viewing the plasma at the snake radius r_S, at the inversion radius r_{inv} (a few cm inside $r_{q=1}$) and at a radius larger than r_{inv}. Note that a similar value for $r_{q=1}$ is deduced from the ablation dip on the H_α signal monitoring the pellet ablation[8,9]. The difference between $r_S = 0.14 \pm 0.015$ m and $r_{q=1} = 0.29 \pm 0.015$ m clearly indicates that the snake rotates on a surface well inside the q=1 surface. Since it has a m=1 n=1 helicity, this implies that a second q=1 surface is present at $r = r_S$: that is the q profile is flat or non-monotonic. This may also explain the survival of the snake to the crashes: as for partial or localized sawteeth, crashes affect only a small annular region around the most external q=1 surface[11]. The possibility of a q profile with two q=1 surfaces is also in agreement with the fact that double snakes have been observed on JET [3]. For the experimental conditions mentioned above, all the snakes verify the relation $r_S/r_{q=1} \approx 0.5$. For comparison, snakes obtained in other experimental conditions have $r_S/r_{q=1} \approx 0.8$ and they also survive to several crashes. In this latter case, the existence of a non-monotonic q profile is less clear.

As already said, snakes survive to sawtooth crashes, but their "regular" evolution is perturbed at the crash time. Figure 5 (top) shows that the snake radius r_S decreases in correlation with the crashes from 0.14 ± 0.15 m down to 0.10 ± 0.15 m. This appears at the bottom of Figure 5, where the central soft X-ray brightness is shown, exhibiting an

inverted sawtooth. When r_s decreases, the snake rotates on a trajectory more inside always intercepted by the central vertical chord. As a consequence of the conservation of the snake particles and of the smaller dimensions, the central soft X-ray brightness increases. During the sawtooth quiescent phase r_s recovers rapidly, much more rapidly than in JET [3], where the same sudden r_s reduction has been observed.

The snake rotation frequency varies during its lifetime (Figure 6). Generally on Tore-Supra, the time evolution of the snake rotation can be split into two components. The first one, with a slow time scale, corresponds to an increase of the frequency from about 0 at birth to 600 Hz at the end of the snake, whereas the second one, much more rapid, is superimposed to the previous one and is induced by the sawteeth. Each crash corresponds to an abrupt decrease, of the order of 300 Hz, of the snake rotation frequency. When the snake frequency is low, this effect leads to a reversal of the rotation direction from the electron to the ion diamagnetic drift direction. During the following sawtooth recovery the frequency decreases, locks and reverses. It must be pointed out that when a typical m=1, n=1 tearing mode is observed during the sawtooth activity, it has a rotation frequency evolution different from that of the snake: it slows down before the crash, whereas the m=1, n=1 snake slows down at the crash.

2-c Snake and current profile

Three different methods have been used to verify the hypothesis of a second q=1 surface (i.e. the presence of shear reversal or of a q "plateau"), which is necessary to explain the fact that the snake rotates inside the q=1 surface:

1. the q profile is obtained from Thomson scattering and magnetic data. They have been fitted using the Spitzer's resistivity (for Tore-Supra, this tends to underestimate the current density on the axis [12]). The bootstrap current contribution has been evaluated using Rosenbluth et al. expression[13],

2. the equilibrium code IDENT-D [14], using magnetic probe and interferometer data, together with the q=1 surface position from the sawtooth inversion radius,

3. the striations on the H_α emission during pellet ablation [15].

Figure 7 shows the q profiles obtained by these three methods. Before pellet injection, the results are in relatively good agreement, showing a monotonic q profile with a central value $q(0) = 0.85 \pm 0.15$. The profile obtained from the striations indicates the presence of a large plateau around $r_{q=1}$, but no particular structure around the snake radius r_s.

After the pellet injection, the first method gives a non-monotonic q profile, due to a very flat or even hollow temperature profile, but the large errors and the very poor spatial resolution of the measurements make this result uncertain. The bootstrap current j_{bs}, evaluated before the pellet and during the snake, is shown in Figure 8. During the snake lifetime, its maximum is located between r_s and $r_{q=1}$, i.e., more inwards than

before pellet injection. The integrated value of the bootstrap current is constant at approximately 70 kA, i.e., about 5% of the total Ip. Finally, it has been impossible to calculate the q profile after pellet injection from the equilibrium code IDENT-D, because of convergence problems.

3. EVALUATION OF THE SNAKE ELECTRON DENSITY AND OF THE IMPURITY CONTENT

On Tore-Supra, the average effective charge Z_{eff} is routinely obtained from quantitative analysis of the visible bremsstrahlung emission at a wavelength around 5238 Å. For more detailed investigations, the impurity content is obtained by using an impurity transport code simulating simultaneously all available experimental data (XUV line spectroscopy, soft X-ray emission and visible bremsstrahlung) [16]. The atomic physics data needed to describe ionisation, recombination and both line and continuum emission are reviewed in Ref.[17]. For quantitative simulations of the snake, it is necessary to have an absolute calibration of the soft X-ray signals; the detector sensitivity has been roughly estimated from the manufacturer data and empirically corrected to agree with the numerical simulations in a variety of experimental situations with soft X-ray signals of quite different levels [16].

Prior to pellet injection, this quantitative analysis gives a central value of the effective charge $Z_{eff}(0) = 1.40 \pm 0.05$, due to a central carbon density $n_C(0)$ of approximately $4.5\ 10^{17}\ m^{-3}$. Pollution by oxygen, chlorine and heavy metals (mainly Fe) is negligible. The simulations indicate that approximately one half of the soft X-ray emissivity is due to carbon, the second half being due to deuterium. During the snake lifetime, the corresponding simulations are less accurate. Both visible bremsstrahlung emission and the C VI Lyman-α line (the most interior C line, necessary to deduce the C content) have insufficient time resolution to follow the Z_{eff} and C content evolutions during the post pellet injection phase. The effective charge Z_{eff} is close to one, with an increased weight of its absolute error. The $n_e(r)$ profile cannot be obtained using the standard Abel inversion procedure, since the modulations of the line integrated densities do not have a m=0 helicity. Therefore, the modulations due to the snake are first neglected. An iterative procedure is used to obtain the unperturbed $n_e(r)$ profiles, by minimizing the deviations of the line integrated densities from the experimental minima of the five interferometer channels, using reflectometry data as peripheral boundary condition. Similarly, the modulations due to the snake on the soft X-ray camera signals are neglected to simulate the unperturbed plasma. Snake simulations are performed at three times (8.60, 8.68 and 8.87 s), giving estimated values of $Z_{eff}(0)$ and $n_C(0)$ equal, respectively, to 1.02, 1.05, 1.10 and to $1.\ 10^{17}$, $1.5\ 10^{17}$, $2.2\ 10^{17}\ m^{-3}$. The simulated

soft X-ray emissivity is dominated by D/H ions, C ions contributing at maximum by 20% at the third time.

The snake has been simulated as an off-axis perturbation superposed to the unperturbed, previously simulated plasma which is well centred on the magnetic axis R_0. The circular perturbation rotates without deformation around the magnetic axis. $R_0 = 2.40$ m is obtained from the magnetic equilibrium (Shafranov's shift included) and its position is verified at each time by the correctly centred simulation of the unperturbed soft X-ray brightnesses. The centre of the snake (R_S,H_S) is given with respect to a R, H coordinate axis (R is the major radius and H the height with respect the equatorial plane). It intercepts the unperturbed plasma on a magnetic surface of radius r_S. The snake electron density profile, $n_{es}(\rho_S)$, is supposed parabolic with a maximum value $n_{es}(0)$ and with zero value at a radius ρ_S equal to the snake radius a_S. To begin with, by rotating the snake on a magnetic surface of radius r_S, the interferometer modulation are simulated by a suitable choice of $n_{es}(0)$, a_S and r_S. Subsequently, to simulate the soft X-ray brightnesses it is necessary to specify both the snake electron temperature T_{es} and the snake impurity content. T_{es} is taken constant in the snake and equal to $T_e(r_S)$ (obtained from ECE Fabry-Perot and Michelson interferometer data); carbon is considered as the only impurity, with constant concentration inside the electron density perturbation superposed to the unperturbed plasma.

Figure 9 shows four simulations at four positions during a snake rotation (t=8.68 s), as seen on the soft X-rays. The simulation of the snake electron density (not shown) gives $n_{es}(0) = 5.\ 10^{19}$ m^{-3}, $a_S = 0.23$ m and $r_S = 0.13$ m. From left to right, the snake is at the interior ($R_S = 2.28$ m, $H_S = 0$ m), at its upper position ($R_S = 2.40$ m, $H_S = 0.13$ m), at the exterior ($R_S = 2.53$ m, $H_S = 0$ m), and at its lower position ($R_S = 2.40$ m, $H_S = -0.13$ m). The soft X-ray brightnesses (W/cm^2/sr) are given as functions of a spatial coordinate corresponding to the intersection of the viewing chords with the equatorial plane (in m). At the same time, for the base plasma $n_e(0) = 1.\ 10^{20}$ m^{-3}, $T_e(r_S) \leq T_e(0) \approx 1.1$ keV. The stars show the experimental soft X-ray brightness profiles, the dashed lines show the simulations of the unperturbed base plasma, whereas the dot-dashed lines show the simulations assuming a C concentration inside the perturbation equal to that of the unperturbed plasma. It appears clearly that, with this assumption on the C concentration, it is not possible to simulate the snake oscillations on soft X-rays; therefore it is necessary to increase the carbon concentration inside the perturbation. The solid lines show the final simulations. The central C density in the perturbation, superposed on the unperturbed plasma, increases from $7.5\ 10^{16}$ m^{-3} up to $1.7\ 10^{18}$ m^{-3} with a final Z_{eff} value inside the snake (parabolic density perturbation plus base plasma) of about 1.36. Simulations have also been performed to check the influence of an error on the T_e evaluation as well as the influence of a heavy impurity. The effective

excitation rates for soft X-ray emission are an increasing function of T_e, and are larger for a heavy element like Fe than for light elements. If one takes T_e inside the snake 0.9 times smaller than T_e outside the snake, the central C density in the perturbation and the Z_{eff} in the snake must be increased, respectively, to 2. 10^{18} m^{-3} and to 1.4 to simulate the experimental data. Similarly, assuming inside the snake a Fe density of the order of 1 10^{15} m^{-3} (an upper limit) the same two parameters become 1.5 10^{18} m^{-3} and 1.34. The presence of a Fe density of the order of 1 10^{15} m^{-3} should be observed by the XUV spectrometer line emission, but this is not the case.

Figure 10 is the same as Figure 9, but at 8.87 s. Now the simulation of the snake electron density has given $n_{es}(0) = 5.\ 10^{19}$ m^{-3}, $a_s = 0.17$ m and $r_s = 0.125$ m. From left to right the snake is at the interior ($R_s = 2.28$ m, $H_s = 0$ m), at its upper position ($R_s = 2.40$ m, $H_s = 0.125$ m), at the exterior ($R_s = 2.52$ m, $H_s = 0$ m), and at its lower position ($R_s = 2.40$ m, $H_s = -0.125$ m). At the same time, for the base plasma, $n_e(0) = 7.\ 10^{19} m^{-3}$, $T_e(r_s) \leq T_e(0) \approx 1.5$ keV. In this case, to obtain the final simulations it is necessary to increase the C density in the perturbation from 1.5 10^{17} m^{-3} up to 4. 10^{18} m^{-3}, with a final Z_{eff} value inside the snake of about 2.1. Other simulations have shown that during the snake decay this latter value does not change. For the simulations shown in Figure 10, with smaller snake dimensions it is not possible to simulate the bump seen on the interior when the snake is on its external position. This is also the case when the snake is on its internal position and the bump on the external side is slightly smaller. This disagreement is probably a consequence of the simplicity of our model, considering an unperturbed well centred plasma with a superposed circular snake perturbation rotating without deformation around the magnetic axis. It is quite likely that the observed experimental bumps are associated with perturbations of the magnetic surfaces causing a displacement of the hot plasma outside the snake in a direction opposite to it. To verify this hypothesis a more refined data analysis is required. Clearly the first idea is to apply tomographic techniques. These require at least two soft X-ray cameras and, moreover, are difficult to apply when the perturbations are located near the magnetic axis. Another possibility is the technique of cartography of the magnetic surfaces (or rather of the soft X-ray isoemissivity surfaces) employed in the past on the TFR Tokamak [18]. Once the tomographic inversion or the cartography are performed, a model with hypothesis on n_e, T_e and the impurity content will be necessary to recover interferometric, soft X-ray, and possibly ECE data.

The simulations shown in Figs 9 and 10 indicate that when the snake oscillations are clearly developed on the soft X-ray signals (i.e., at t larger than 8.65 s) the impurity (carbon) density inside the snake is much larger than outside it. What is happening previously to this time, as far as the carbon content inside the snake is concerned, is less clear. The interferometer data show that the snake appears soon after the injection when

the soft X-ray signals are low as a consequence of the pellet induced cooling. We have, therefore performed a third simulation, at 8.60 s, when $n_e(0) \leq 1.2\ 10^{20}\ m^{-3}$ and $T_e(0) \approx$ 0.85 keV. Since no oscillations are seen on the soft X-rays and the n_e oscillations are visible only on three interferometer channels, there is quite a latitude in the choice of the snake parameters to simulate a central line integrated electron density modulation of approximately $1.\ 10^{19}\ m^{-2}$, one of these possibilities being $n_{es}(0) = 4.10^{19}\ m^{-3}$, $a_s = 0.24$ m and $r_s \approx 0.10$ -0.12 m. The noise level on the soft X-ray data is so large that even a central C density of about $8.\ 10^{17}\ m^{-3}$ (implying a snake effective charge Z_{eff} of about 1.2) does not show snake oscillations above it. Therefore, no firm conclusion can be drawn on the carbon content inside the snake during the first 80 milliseconds of its lifetime. However, a change of regime, with subsequent carbon accumulation inside the snake, seems quite possible around 8.65 s, since Fig. 1 shows that the amplitude of the the soft X-ray signal modulations increases regularly between 8.65 s and 8.70 s, and they are not distinguishable previously.

4. THEORETICAL CONSIDERATIONS

4-a Formation of the snake

The Tore-Supra data do not disagree with the hypothesis of snake formation caused by a localized current drop on the q=1 surface, as in the model proposed by Wesson [5]. This current depletion should appear during the ablation process, due to the topology of the closed field lines on q=1. Thus it is probably localized in the flux tube intercepted by the pellet and should exhibit an m=1 n=1 helicity. As a consequence, a magnetic island is formed which traps some of the particles released from the pellet, thus forming the snake. However, the fact that, in the presence of shear reversal or "plateau", a snake is formed only inside the q=1 surface could be associated with a preferred ablation and cooling on this second, internal, q=1 surface, apparing just at the ablation time.

4-b Stability criteria

The presence of the snake, which we suppose to be a m=1 n=1 island, changes the magnetic field topology. It induces both an ohmic current, described by Rutherford's theory [19], and an island bootstrap current, associated with the large pressure gradients outside and inside the island. As described before, soft X-ray analysis shows carbon accumulation within the snake, thus also leading to a current which contributes to the stability. Thus, there are two additional mechanisms likely to drive the snake:

-the variation of resistivity inside the snake due to the carbon content increase [5].

-the modification of the bootstrap current induced by the presence of a large m=1, n=1 island snake perturbation [20].

The problem is to evaluate the contribution of each effect in terms of Δ', the discontinuity of the vector potential amplitude, across the resonant layer. For simplicity, we assume a monotonic current profile, consider the snake as an island of m=1, n=1 helicity, and also neglect coupling terms with other modes. The calculation is carried out within the Rutherford's theory which is not exact for a m=1 n=1 mode, nevertheless it leads to a qualitative approach for the stability study. With the traditional assumptions of a slowly varying perturbation of the vector potential $\tilde{A}_{//}$ inside the resonant layer and of a leading role of the m=1, n=1 component over the other terms, the qualitative time evolution of the half island size δ_s is then given by the non linear equation:

$$\frac{\partial \delta_s}{\partial t} = \frac{1}{k_1}\frac{\eta}{\mu_0}\left[\Delta' + \Delta'_{\eta} + \Delta'_{jbs}\right] \qquad (1)$$

where k_1=1.7, η is resistivity. For a finite shear, Δ' is given by the Bussac et al.[21] formula and depends on pressure and current profiles. In the case of a shear plateau, the formula of De Blank et al.[22] must be used. In principle, Δ' can be modified by diamagnetic and other effects.

***Bootstrap contribution:** Δ'_{jbs}

The Arnpere law for the bootstrap contribution leads to:

$$\Delta'_{jbs}\tilde{A}_{//} = \mu_0 \int_{-\infty}^{+\infty}\int_{-\alpha_0}^{+\alpha_0} \frac{d\alpha}{2\pi} j_{bs}(r,\alpha)\cos\alpha \; dr \qquad (2)$$

for the island bootstrap current j_{bs} we use the expression calculated by Carrera[23]:

$$j_{bs} = -1.46\sqrt{\varepsilon_s}\frac{R_s T_s}{4}\frac{q_s}{q'_s}\frac{\delta_s}{S(\overline{\Psi})}\frac{\partial n}{\partial \overline{\Psi}}\theta(\overline{\Psi}-1) \qquad (3)$$

with:

$\varepsilon_s = r_s/R_s$ $\quad$ R_s major radius $\quad$ T_s the snake temperature

q_s safety factor on r_s $\quad$ $q'_s = dq/dr$ at $r=r_s$

$\overline{\Psi}$ the normalised poloidal flux defined by $\overline{\Psi} = \Psi / 2\tilde{A}_{//}R$

$$S(\overline{\Psi}) = 1/2\sqrt{2}\int_{-\alpha_0}^{\alpha_0} 1/\sqrt{\overline{\Psi}-\cos\alpha}\; d\alpha/2\pi$$

α is the angle related to the helicity, α_0 and-α_0 correspond to the X point of the island

From symmetry considerations over the perturbed magnetic flux lines, it can be shown that the bootstrap current averaged over the island is zero, in spite of the large density gradients. Thus, only its perturbation induced by the presence of a large m=1, n=1 snake island has to be taken into account. This property is illustrated in formula 3 by the function $\theta(\overline{\Psi}-1)$, which is zero for $\overline{\Psi}$ varying from -1 to 1, corresponding to the domain inside the island.

Using (3) for the snake leads to the relation:

$$\Delta'_{jbs} = 1.15\sqrt{\varepsilon_s}\beta_p \frac{1}{L_n}\frac{r_s}{s_s}\frac{1}{\delta_s} \qquad (4)$$

where: β_p is poloidal beta defined on r_s

L_n is the density length decrease calculated faraway from the resonance

s_s is the shear value at the resonance.

***Impurity contribution:** Δ'_η

In the same way, one has:

$$\Delta'_\eta = \mu_0 J_{s//} \int_{-\infty}^{+\infty} \int_{-\alpha_0}^{+\alpha_0} \frac{d\alpha}{2\pi} \frac{\delta J_{//}(r,\alpha)}{\tilde{A}_{//} J_{s//}} \cos\alpha \; dr \qquad (5)$$

here $\delta J_{//}(r,\alpha)$ refers to the current perturbation induced by the local impurity accumulation and must be deduced from the δZ_{eff} experimental value. Using the Ampère's law, the parallel equilibrium current $J_{s//}$ on r_s is given by:

$$\mu_0 J_{s//} = \frac{B_\varphi}{R_s}\left(\frac{2}{q_s} - \frac{2s_s}{q_s}\right) \qquad (6)$$

Defining $\rho = (r - r_s)/\delta_s$, so that $\overline{\Psi} = 2\rho^2 + \cos\alpha$, and supposing a parabolic profile for Z_{eff} inside the snake, the relation between $\delta J_{s//}$ and δZ_{eff} is given by:

$$\frac{\delta J_{s//}}{J_{s//}} = -\frac{\delta Z_{eff}}{2 Z_{eff}}\left(1 - \overline{\Psi}\right) \qquad (7)$$

Including (6) and (7) into (5) leads to the following result:

$$\Delta'_\eta = \frac{128}{15\pi} \frac{2 - s_s}{s_s} \frac{\delta Z_{eff}}{Z_{eff}} \frac{1}{\delta_s} \qquad (8)$$

The two terms, bootstrap and impurity, behave in the same way: both are destabilizing effects.

***Global equation:**

Finally the snake time evolution is governed qualitatively by the equation:

$$\frac{\partial \delta_s}{\partial t} = \frac{1}{k_1} \frac{\eta}{\mu_0}\left[\Delta' + 1.15\sqrt{\varepsilon_s}\beta_p \frac{1}{L_n} \frac{r_s}{s_s} \frac{1}{\delta_s} + \frac{128}{15\pi} \frac{2 - s_s}{s_s} \frac{\delta Z_{eff}}{Z_{eff}} \frac{1}{\delta_s}\right] \qquad (9)$$

For the considered case, it is clear that after the initial phase (t>8.64s) of the snake, the impurity term dominates over the current bootstrap one (since $\frac{\delta Z_{eff}}{Z_{eff}} > 8\%$). The latter may contribute to the snake evolution during the initial phase, but once again it must be compared to other additional contributions, such as the diamagnetism or the change of resistivity induced by the local cooling.

However, no clear conclusions can be drawn since the Δ' and shear terms are not known. If we consider the saturation phase, the stability, in the limits of this simplified model, is determined (using (9)) by:

$$\Delta' r_s = -\frac{128}{15\pi} \frac{\delta Z_{eff}}{Z_{eff}} \frac{r_s}{\delta_s} \frac{2 - s_s}{s_s}$$

This gives for Tore-Supra $\Delta' r_s = -6\,\frac{2-s_s}{s_s} \cong -\frac{12}{s_s}$

For a flat q profile, i.e., a low value of s_s, this means that Δ' is strongly negative. This suggests the presence of stabilizing effects.

4-c Confinement in the snake

Following Wesson's notation [5] we find $n_{Cs}/n_{C0} = (n_{Hs}/n_{H0})^{6\phi} \approx$ 20-30. The subscripts s and 0 refer to snake and background plasma respectively. ϕ is a factor to allow for uncertain anomalous transport processes, which is of order of magnitude of unity. This impurity accumulation increases the resistivity maintaining the magnetic island. It does not seem necessary to invoke the second process considered by Wesson [5], to explain the persistence of the density perturbation , i.e., a modification of the local confinement (through increased pinch velocity) in the magnetic island increasing the density. This is justified by the fact that for Tore-Supra, the snake lifetime is of the same order as of that particles (600ms) deduced from the central electron density.

5. CONCLUSION

Snakes observed in Tore-Supra, after injection of high velocity solid hydrogen pellets ablated inside the q=1 surface, have been described. There is broad agreement with previously reported data from other Tokamaks, essentially JET, with nevertheless one important difference. It concerns the fact that in several pellet injections the snake radius r_s is clearly smaller than the q=1 surface radius $r_{q=1}$, deduced from the sawtooth inversion radius. This is interpreted in terms of a very low or even reversal shear, with the inclusion of a bootstrap current of the order of 5% of the total plasma current.

The snake density is deduced from the interferometer line electron density modulations. Quantitative analysis of the soft X-ray brightnesses has indicated that, when the modulations due to the snake are fully developed, the impurity carbon density inside the snake is much larger than in the background plasma, implying Z_{eff} values inside the snake of 1.35 at t = 8.68s, increasing up to about 2 at t = 8.88 s (i.e., respectively 120 and 320 ms after the pellet injection and the almost simultaneous snake appearance). During the first 100 ms after the injection the snake is seen only on the line electron densities. The soft X-ray signals (decreased as a consequence of the pellet induced cooling) do not show snake modulations above the noise level. No conclusion can be drawn about impurity (carbon) accumulation in the snake during this phase, but the facts that the soft X-ray oscillations appear around t = 8.64 s (see Figure 1) and that they seem to develop quite suddenly rather than progressively point towards an absence of impurity (carbon) accumulation inside the snake in the initial phase of its evolution.

By locally changing the resistivity, the carbon acculation contributes to the stability of the snake. The time evolution of the snake size is obtained from a simple model considering a monotonic q profile. It shows that the impurity and bootstrap contributions are destabilising effects and that after the initial phase, when $\delta Z_{eff}/Z_{eff}$ is greater than approximately 10%, the impurity contribution dominates the bootstrap one.In the case of low shear, i.e., flat q profile on the resonant surface, the Δ' is strongly negative, suggesting the presence of stabilizing effects.

Further experiments are needed (in particular, infrared polarimetry data and more accurate density and temperature measurements) to estimate the current profile modification induced by the pellet, and also it is necessary to take into account the ablation process and impurity accumulation to model the snake creation and stability.

ACKNOWLEDGEMENTS

It is a pleasure to thank M.A. Dubois and G.T. Hoang for useful discussions as well as D. Garnier for his technical support. The authors wish also to express their appreciation to the Tore-Supra operating team.

REFERENCES

[1] WELLER A., CHEETHAM A. D., EDWARDS A. W., et al., Phys. Rev. Lett. 59(1987) 2303.

[2] MILORA S.I.,HOULBERG W.A., LENGYEL L.L. and MERTENS W., Nucl. Fusion 35 (1995) 657.

[3] GILL R. D., EDWARDS A. W., PASINI D. and WELLER A., Nucl. Fusion 32 (1992) 723.

[4] GILL R.D., ALPER B., EDWARDS A.W. and PEARSON D in Controlled Fusion and Plasma Physics (Proc. 21th Eur. Conf. Montpellier) ,Vol 18B, Part I, European Physical Society, Geneva (1994)198.

[5] WESSON J., Plasma Phys. Control. Fusion 37 (1995) A337.

[6] CRISTOFANI P., DESGRANGES C., GARBET X., et al. in Controlled Fusion and Plasma Physics (Proc. 21th Eur. Conf. Montpellier) ,Vol 18B, Part I, European Physical Society, Geneva (1994) 210.

[7] GERAUD A., CHATELIER M., DRAWIN H.W., et al. in Controlled Fusion and Plasma Physics (Proc. 20th Eur. Conf. Lisboa) ,Vol 17C, Part I, European Physical Society, Geneva (1993)163.

[8] GILL R. D., EDWARDS A. W. and WELLER A., Nucl. Fusion 29 (1989) 821.

[9] PEGOURIE B. and DUBOIS M.A. Nucl. Fusion 30 (1990) 1575.

[10] DUDOK de WIT T., PECQUET A.L., VALLET J.C. and LIMA R., Phys. Plasmas 1 (1994) 3288.
[11] EDERY D., PECQUET A.L., CRISTOFANI P., et al. in Controlled Fusion and Plasma Physics (Proc. 20th Eur. Conf. Lisboa) ,Vol 17C, Part IV, European Physical Society, Geneva (1993)1303.
[12] HARRIS G.R., CAPES H. and GARBET X., Nucl. Fusion 32 (1992) 1967.
[13] ROSENBLUTH M.N., HAZELTINE R.D., HINTON F.L., Phys. Fluids 15 (1972) 116
[14] BLUM J.,LAZZARO E.,O'ROURKE J., et al., Nucl. Fusion 30 (1990) 1475.
[15] DUBOIS M.A., SABOT R., PEGOURIE B., et al. Nucl. Fusion 32 (1992) 1935.
[16] GUIRLET R., MATTIOLI M., DE MICHELIS C., et al. in Controlled Fusion and Plasma Physics (Proc. 21th Eur. Conf. Montpellier) ,Vol 18B, Part III, European Physical Society, Geneva (1994)1280.
[17] MATTIOLI M., DE MICHELIS C., MONIER-GARBET P., et al."Laser Blow-off Injection of Metal Impurities in Tore Supra", (1993) Rep. EUR-CEA-FC 1491 CEN Cadarache (unpublished).
[18] DUBOIS M.A., MARTY D.A. and POCHELON A., Nucl. Fusion 20 (19) 1335.
[19] RUTHERFORD P.H., Phys.Fluids 16, (1973)1903.
[20] THYAGARAJA A. and HAAS F.A., in Controlled Fusion and Plasma Physics (Proc. 20th Eur. Conf. Lisboa) ,Vol 17C, Part IV, European Physical Society, Geneva (1993)1323.
[21] BUSSAC M.N., et al., Phys. Rev. Lett., 35 (1975) 1638.
[22] DE BLANK H.J. and SCHEP T.J., Phys. Fluids, B3 (1991) 1136.
[23] CARRERA R., HAZELTINE R.D. and KOTSCHENREUTER M., Phys. Fluids 29 (1986) 899.

FIGURE CAPTIONS

Fig.1a Electron density (from laser interferometer), electron temperature (from ECE emission) and soft X-ray time evolution during the snake lifetime. One of the two soft X-ray detectors monitors the snake viewing the intersection of the snake with the equatorial plane towards outside, whereas the other monitors the inverted sawteeth viewing the region outside the q=1 surface. The ECE signal monitors the central T_e value. The two interferometer channels cross the plasma on opposite sides with respect to magnetic axis.

Fig.1b Oscillating electron temperature (from Fabry-Perot interferometer) at the early phase of the snake and time evolution of the centralline integrated line electron density as reference.

Fig.2 First two k=1 and k=2 chronos and topos of the biorthogonal decomposition of the soft X-ray diodes time evolutions. The abscissae are, respectively, the time and the intersection of the viewing chord with the equatorial plane.

Fig.3 Sketch of the snake geometry: dimensions and positioning with respect to the magnetic geometry (magnetic axis, centre of the last closed magnetic surface and q=1 surface).

Fig.4 Three soft X-ray diodes are shown with indicated suitable lines of sight for the determination of the q=1 surface.

Fig 5 Sawtooth effect on the snake radius. The snake radius is shown along with a soft X-ray diode signal viewing vertically the plasma.

Fig.6 Snake frequency as a function of the time showing the influence of the sawtooth crashes visible on the soft X-ray bottom signal.

Fig.7 Profiles of the safety factor q as derived from the Spitzer's resistivity calculation before(o–o) and after (solid lines) pellet injection, from IDENT-D (dotted line with Δ) and from the Hα striations.

Fig.8 Bootstrap current profiles before and after pellet injection (dotted and solid lines, respectively).

Fig.9 Simulations of the snake rotation at t=8.68 s as seen on soft X-rays. From left to right and from top to bottom the snake is at the interior, at its upper position, at the exterior and at its lower position. The stars show soft X-ray brightnesses (in $W/cm^2/sr$) are given as function of a spatial coordinate (the intersection of the viewing chords with the equatorial plane in m). The dashed lines show the simulations of the unperturbed base plasma emission, the dot-dashed lines show the effect of adding the snake emission with the same C concentration as in the base plasma. Finally the solid lines show the final simulations with increased C content.

Fig.10 Same as Fig.7 at t=8.87 s.

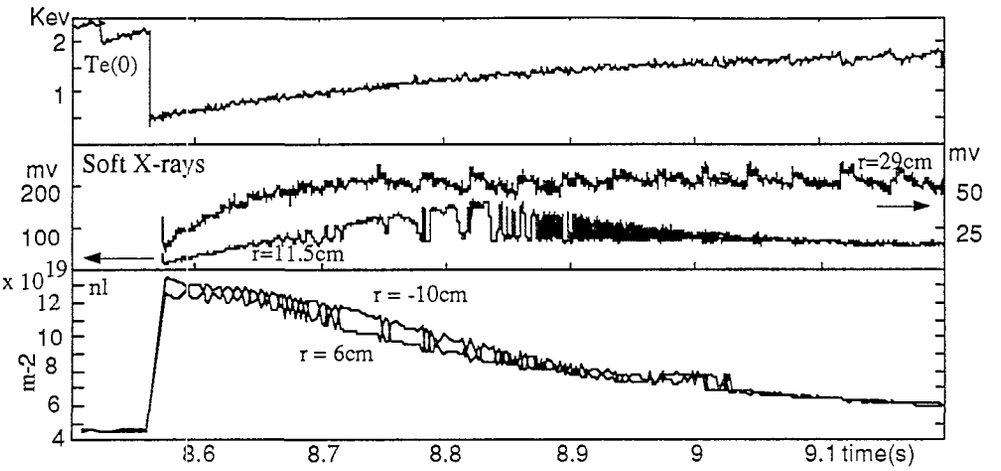

FIG. 1a

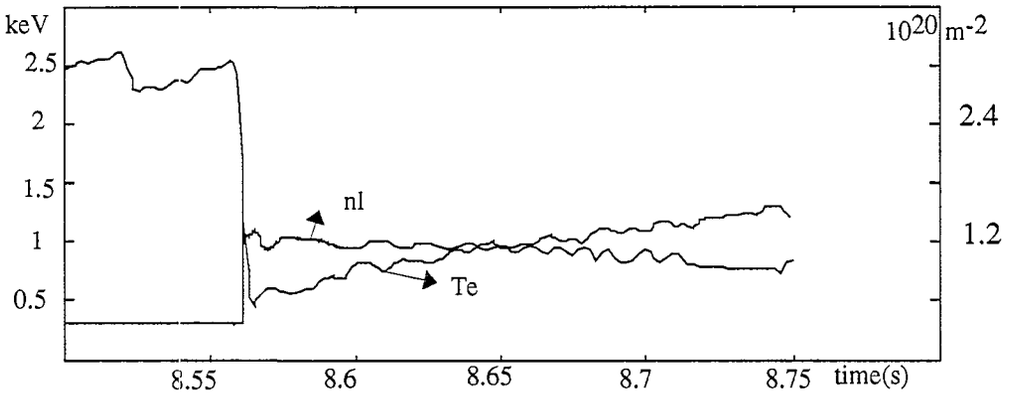

FIG. 1b

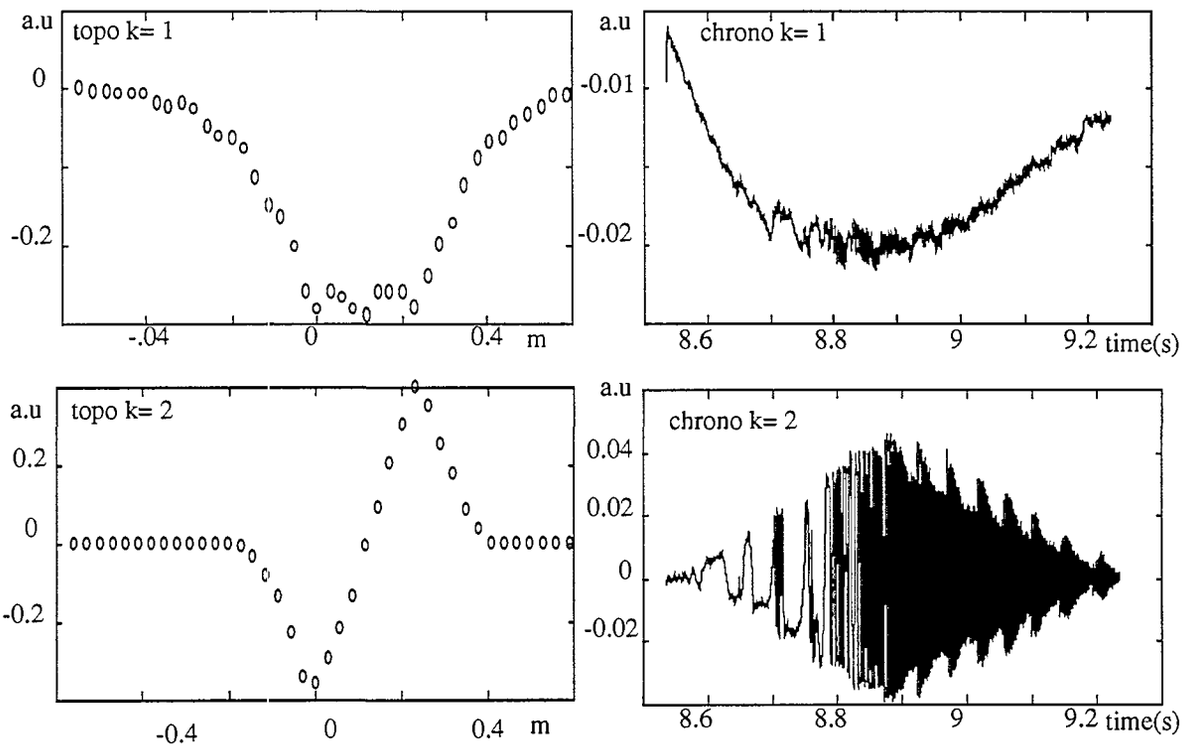

FIG. 2

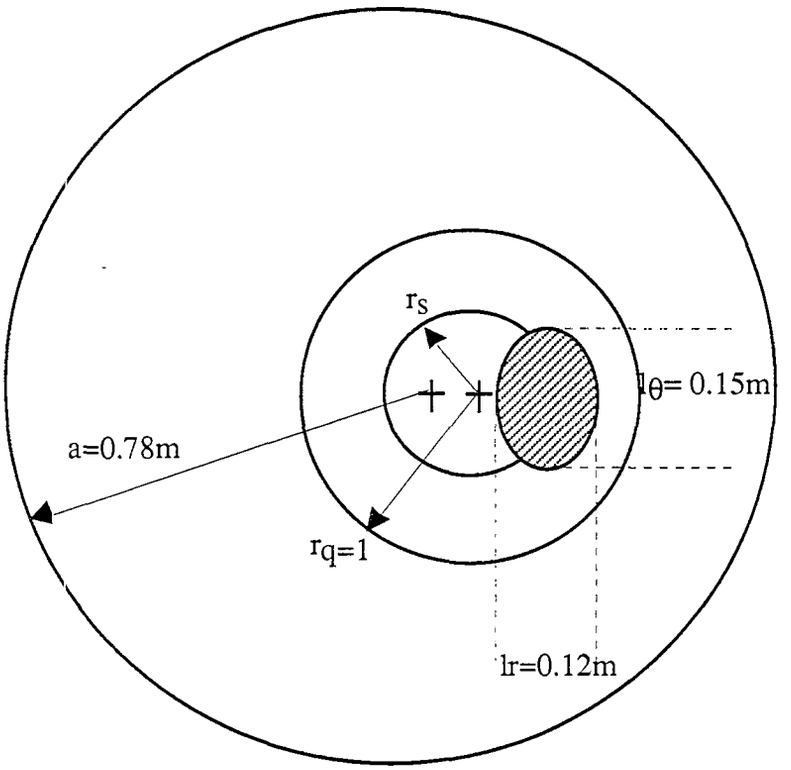
r_s
l_θ= 0.15m
a=0.78m
$r_{q=1}$
lr=0.12m

FIG. 3

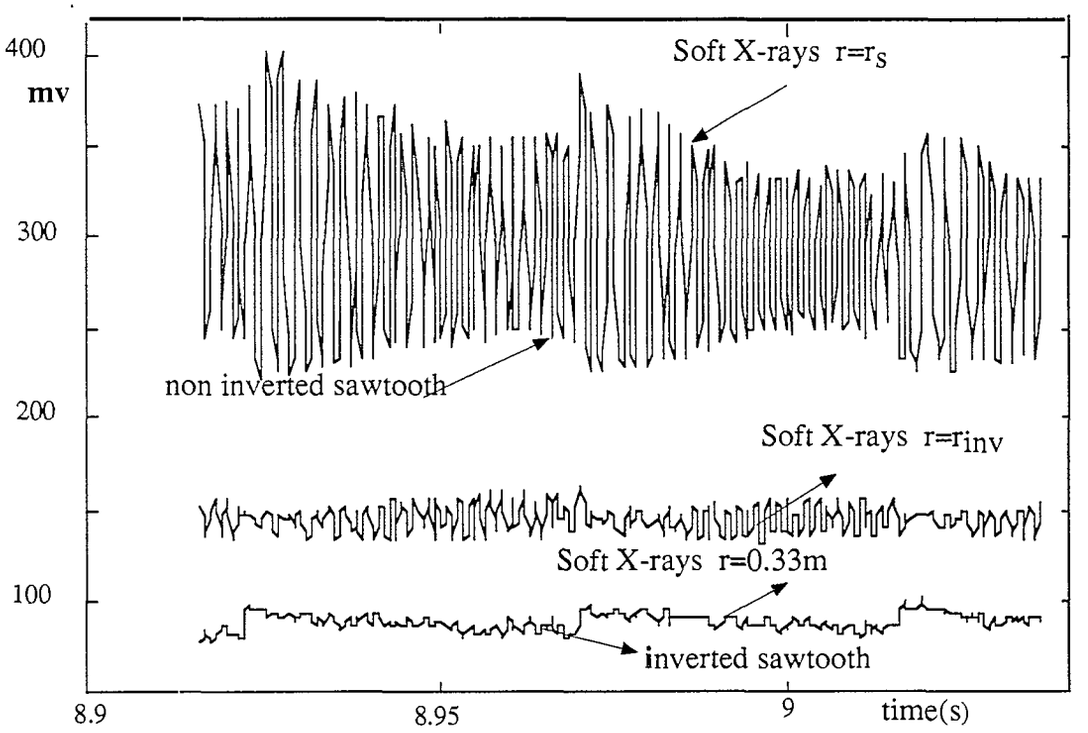
400
mv
300
200
100
Soft X-rays r=r_s
non inverted sawtooth
Soft X-rays r=r_{inv}
Soft X-rays r=0.33m
inverted sawtooth
8.9
8.95
9
time(s)

FIG. 4

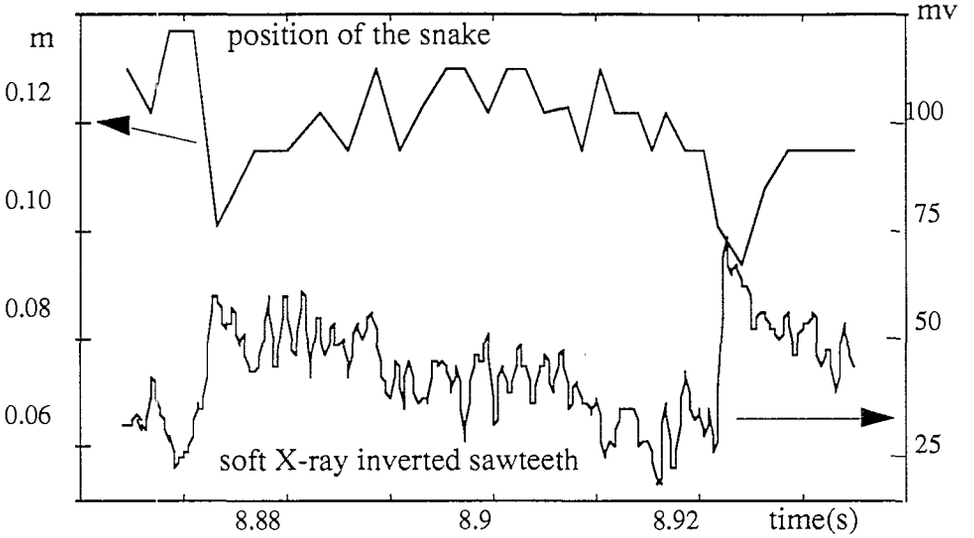

FIG. 5

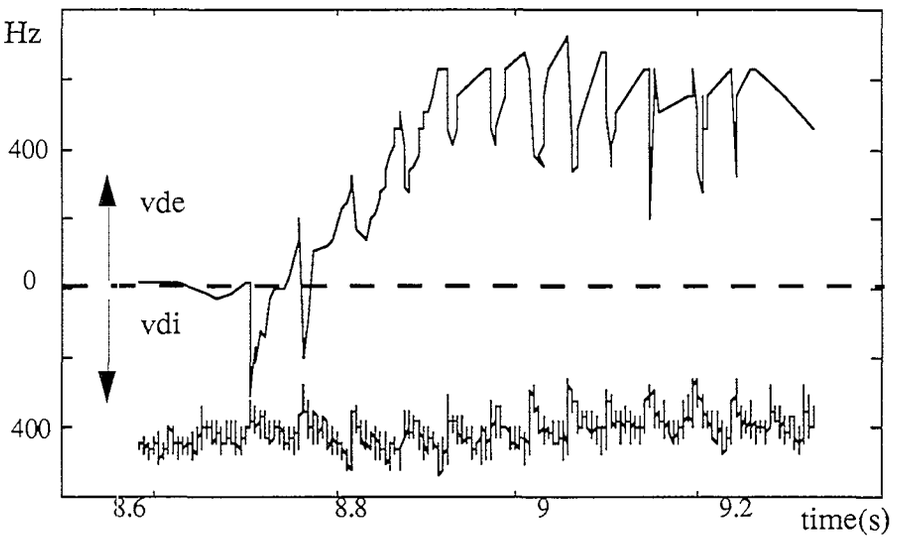

FIG. 6

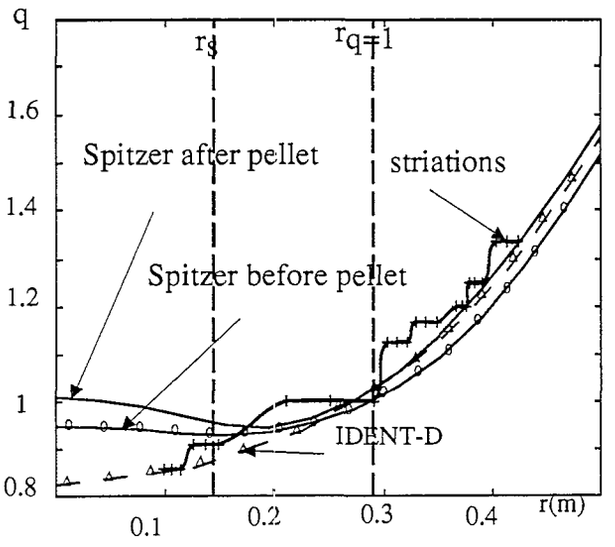

FIG. 7

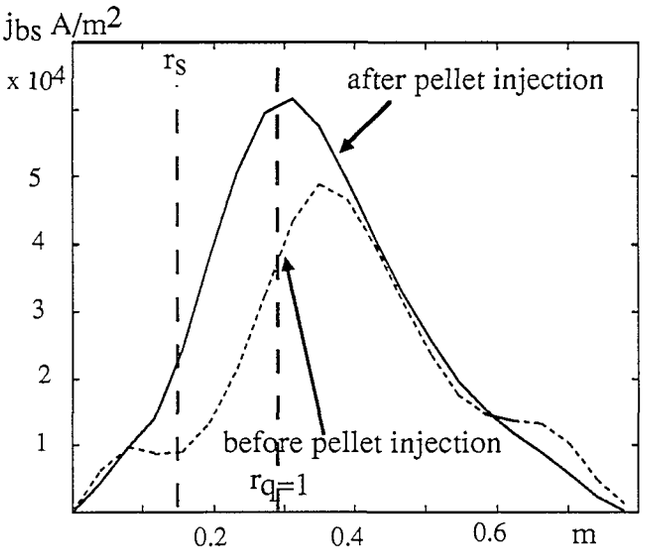

FIG. 8

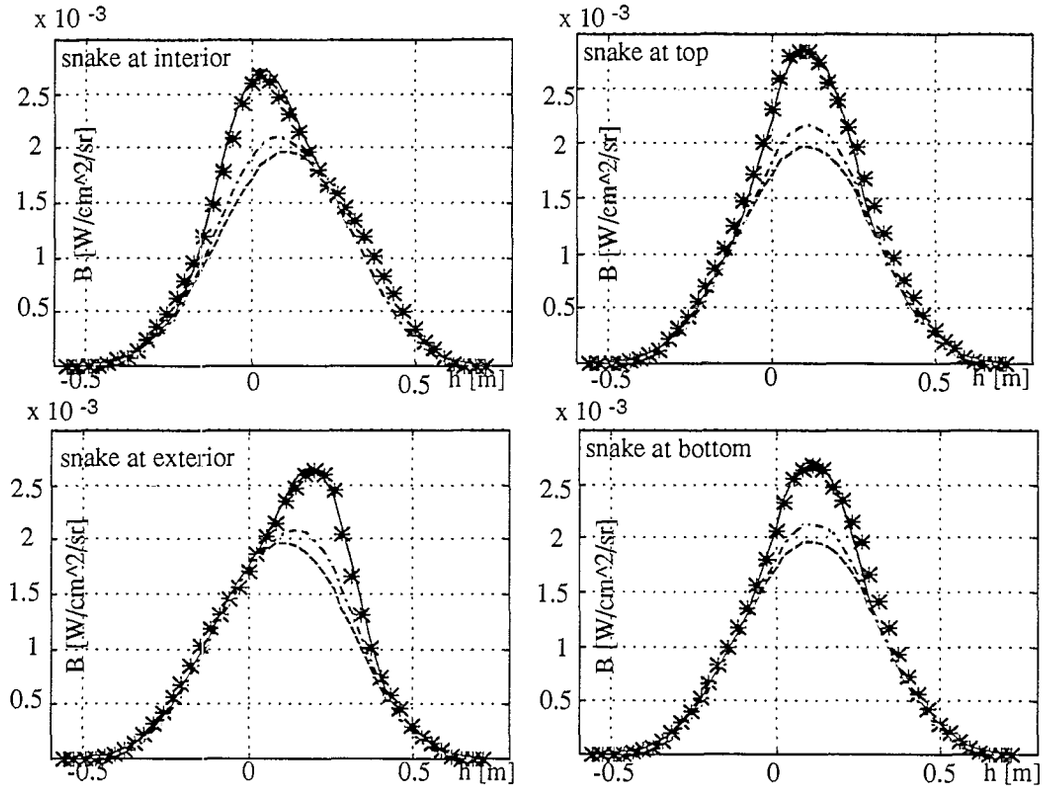
x 10 -3
snake at interior
B [W/cm^2/sr]
h [m]
snake at top
snake at exterior
snake at bottom

FIG. 9

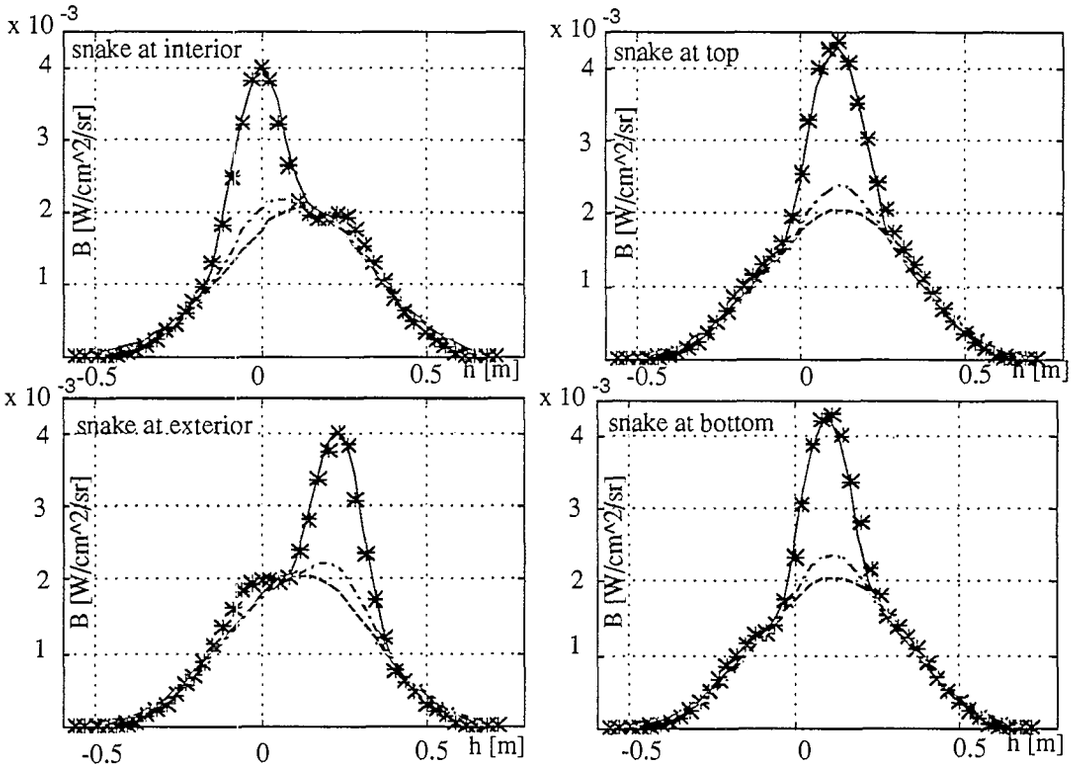
x 10 -3
snake at interior
B [W/cm^2/sr]
h [m]
snake at top
snake at exterior
snake at bottom

FIG.10

Impression Atelier Repro Bâtiment 120 - ☎ 35.49